Electric field tuning of band offsets in transition metal dichalcogenides

Dennis Huang[1] and Efthimios Kaxiras[1,2,*]

[1]*Department of Physics, Harvard University, Cambridge, Massachusetts 02138, USA*
[2]*John A. Paulson School of Engineering and Applied Sciences, Harvard University, Cambridge, Massachusetts 02138, USA*

We use first-principles calculations to investigate the band structure evolution of WX_2/MoX_2 ($X = $ S, Se) heterobilayers under a perpendicular electric field. We characterize the extent to which the type II band alignment in these compounds can be tuned or inverted electrostatically. Our results demonstrate two effects of the stacking configuration. First, different stackings produce different net dipole moments, resulting in band offset variations that are larger than 0.1 eV. Second, based on symmetry constraints that depend on stacking, a perpendicular electric field may hybridize WX_2 and MoX_2 bands that cross at the Brillouin zone corner K. Our results suggest that external electric fields can be used to tune the physics of intralayer and interlayer excitons in heterobilayers of transition metal dichalcogenides.

The richness of properties of the layered compounds known as transition metal dichalcogenides (TMDCs) and the ability to stack individual monolayers, either by mechanical transfer or chemical vapor deposition (CVD), afford several degrees of freedom with which to engineer desired functionalities [1] for a wide range of applications. Single-atomic layers of TMDCs possess a direct band gap in the visible spectrum [2,3] and continue to show promise for many applications that involve electronic excitations, including optoelectronic devices [4]. Of particular interest are heterobilayers of the form WX_2/MoY_2 ($X,Y = $ S, Se), which have staggered, type II band alignment. In most cases, states at the valence and conduction band extrema are localized on the WX_2 and MoY_2 layers, respectively. Photoexcitation can therefore drive charge separation, wherein hot electrons (holes) migrate to the MoY_2 (WX_2) layer [Fig. 1(e)]. Experimentally, ultrafast charge transfer has been observed as a quenching of photoluminescence (PL) signals [5–9] or broadening of reflectance signals [10] from *intralayer* excitons, signaling the dissociation of electron-hole pairs confined to a single layer. Such separation of charge is fundamental to photovoltaic devices [5,11]. In many cases, however, the photoexcited electron and hole on the different layers remained bound as an *interlayer* exciton, giving rise to a new PL signal [12–18]. Although the detailed properties of interlayer excitons have varied with substrate or annealing conditions [8,14,19], the spatial separation of their charges endows them with intrinsic advantages over intralayer excitons. The interlayer excitons have longer radiative [15] and valley [17] lifetimes, such that their diffusion dynamics can be observed. In addition, the interlayer excitons carry an out-of-plane dipole moment that can be coupled to an external electric field [15].

Rivera *et al.* [15] demonstrated that the binding energy of interlayer excitons, as measured by PL, undergoes redshifts or blueshifts depending on the direction of an applied electric field. Within back-gated devices of $WSe_2/MoSe_2$ and $MoSe_2/WSe_2$ on SiO_2/Si substrate, they observed shifts up to 0.06 eV. To first order, they attributed this phenomenon to the electrostatic tuning of band offsets. As a caveat, they noted

that with a single gate, they could not independently adjust electric field and carrier density, the latter also having an effect through screening [20]. Notwithstanding the interpretation of experimental results, it remains crucial to verify theoretically the extent to which an electric field oriented perpendicular to the heterobilayers can modify their band structure features and to elucidate the physics of the induced changes from the fundamental features of the constituents. Such investigations can also provide practical pathways towards realizing excitonic condensates in gate-tunable, double quantum wells of TMDCs [21].

In this work, we use density functional theory (DFT) to examine how the band structure of WX_2/MoX_2 heterobilayers can be tuned by a perpendicular electric field. Previous theoretical studies of electric field effects have focused on TMDC homostructures [22–29] and/or band-gap variations [30,31]; here, we focus on band offsets at the Brillouin zone (BZ) corner K, where direct optical transitions and valley effects prevail. By constructing different stacking registries, we observe variations in the zero-field band offsets larger than 0.1 eV. Our electric field calculations also reveal stacking-dependent hybridization of WX_2 and MoX_2 bands that cross at K, which we explain on the basis of wave function symmetries. We discuss potential implications of all these effects on the physics of intralayer and interlayer excitons as probed by PL experiments.

DFT calculations were performed using the Vienna *ab initio* simulation package (VASP) [32,33], which implements the projector augmented-wave method [34,35]. The valence states are $4s4p5s4d$ for Mo, $5s5p6s5d$ for W, $3s3p$ for S, and $4s4p$ for Se. We used the Perdew-Burke-Ernzerhof (PBE) exchange-correlation functional [36]. To simulate a perpendicular electric field, VASP introduces dipole sheets in the middle of the vacuum regions [37,38], which we took to be larger than 20 Å to avoid interactions between periodic images, making sure that this vacuum size gives well converged energetics and electronic structure features (for details, see the Supplemental Material [39]). For each heterobilayer and for each value of electric field, we performed an ionic relaxation within the supercell. To obtain accurate interlayer distances, we included van der Waals corrections using rescaled C_6 coefficients according to the scheme of Tkatchenko and Scheffler [40],
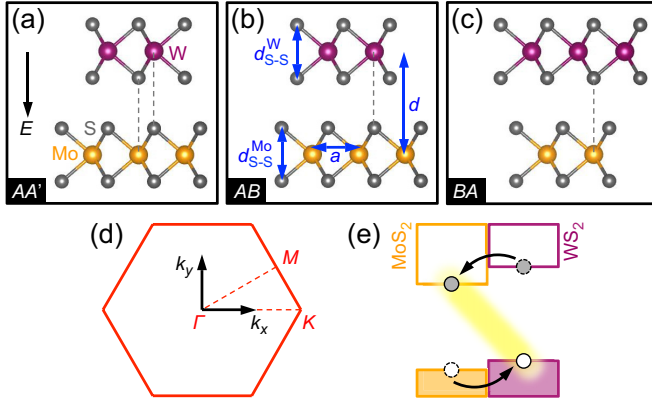
*kaxiras@physics.harvard.edu

FIG. 1. Crystal structures of WS_2/MoS_2 with (a) AA' (180°), (b) AB (0°), and (c) BA (0°) stacking orientations. The black arrow in panel (a) points in the positive direction of the applied electric field, E. (d) Brillouin zone and high-symmetry points corresponding to the 1×1 unit cell. (e) Schematic of the valence and conduction bands in WS_2/MoS_2 with staggered, type II alignment. Upon photoexcitation, the electron and hole are preferentially localized on the MoS_2 and WS_2 layers, respectively, resulting in an interlayer exciton.

with an energy cutoff of 800 eV. Previous calculations of bulk MoS_2 with the Tkatchenko-Scheffler correction produced interlayer distances within 2% of the experimental value [41]. Due to the small dispersion energy, low force tolerances (<0.2 meV/Å) were required for convergence. Following the ionic relaxation, we recalculated the non-spin-polarized charge density on a dense grid ($43 \times 43 \times 1$) of the BZ, and then used it to obtain the wave function with spin-orbit coupling included.

We considered WS_2/MoS_2 and $WSe_2/MoSe_2$ in three stacking configurations, motivated by experimental and theoretical considerations, labeled AA' (180°), AB (0°), and BA (0°) [Figs. 1(a)–1(c)], following the convention of Ref. [42]: Specifically, AA' is fully eclipsed; AB is staggered with W atoms aligned with X atoms of the other layer; and BA is staggered with Mo atoms aligned with X atoms of the other layer [dashed lines in Figs. 1(a)–1(c)]. Although arbitrary twist angles can be achieved by mechanical transfer, interlayer excitons generated at the K/K' valleys are direct for small angles around 0° and 180°, resulting in brighter PL [43]. Furthermore, CVD growth of WS_2 on MoS_2 resulted in AA' stacking [8,14], while similar growth of WSe_2 on

$MoSe_2$ resulted in AA' and AB stackings [16,18]. We restricted ourselves to pure chalcogenide compounds ($X = Y$ in WX_2/MoY_2) in order to minimize strain within a commensurate, 1×1 cell. When optimized, the lattice constants (a) of the heterobilayers deviate at most by 0.3% from the lattice constants of their constituent layers in homobilayer form. Similarly, the interlayer distances (d) of AA'-WX_2/MoX_2 lie within 0.2% of the average between AA'-bilayer WX_2 and AA'-bilayer MoX_2. At the largest electric field considered (5 V/nm), d values change by less than 0.4% of their zero-field values.

Figures 2(a)–2(e) display the band structure evolution of an example heterobilayer, AA'-WS_2/MoS_2, under a perpendicular electric field. High-symmetry points in the BZ are defined in Fig. 1(d). At zero field, AA'-WS_2/MoS_2 exhibits an indirect gap of 1.21 eV. The conduction band minimum at K originates from MoS_2, whereas the valence band maximum at Γ has sizable contributions from WS_2 and MoS_2. However, the valence band at K originates from WS_2, resulting in a type II band alignment at K with a direct gap of 1.35 eV. We compare these results with experimental data acquired by scanning tunneling spectroscopy (STS), which probes the single-particle spectrum without excitonic effects [44]. In a recent measurement of WS_2/MoS_2 and MoS_2/WS_2 transferred onto fused quartz, the single-particle gap observed was 1.45 eV [45]. The MoS_2 conduction band minimum was found to lie at K, whereas it was experimentally uncertain whether the WS_2 valence band maximum resided at K or Γ. Previous theoretical works on AA'-WS_2/MoS_2, using hybrid functionals [46] or single-shot G_0W_0 [47], predicted gap values of 1.60 eV (direct) and 1.96 eV (indirect), respectively (none of these calculations included substrate effects, which are known to be present in the STS measurements). We note that the order of band alignments predicted by PBE and G_0W_0 agree with each other [48].

As the electric field increases [in the direction shown in Fig. 1(a)], there are various nonrigid transformations in the band structure, such as the shifting of the conduction band minimum from K to a midway point along Γ-K. The primary feature of interest for our purposes is the band alignment at K, which becomes inverted beyond 4 V/nm [Fig. 2(e)], as well as the possible hybridization of bands at these crossings. We hereafter focus on the K point, where direct transitions result in bright PL signals [43] and interlayer excitons exhibit valley-polarized dynamics [17].
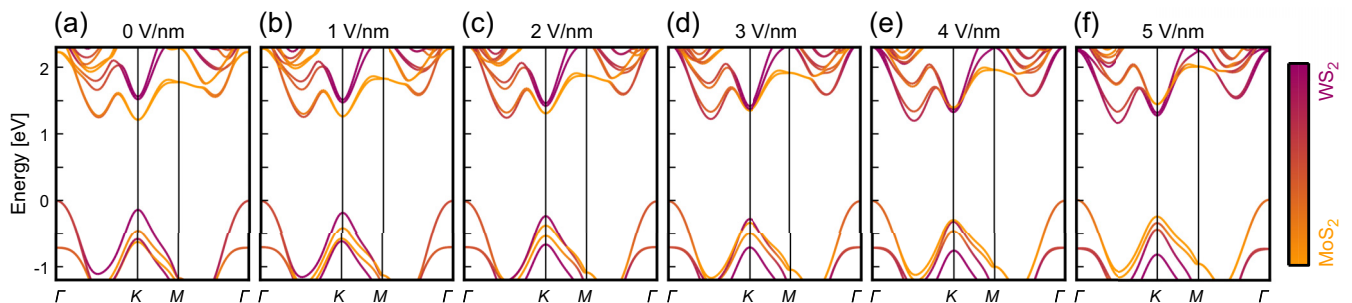

FIG. 2. (a)–(e) Evolution of the band structure of AA'-WS_2/MoS_2 under a perpendicular electric field. The positive direction of the field points from the WS_2 to MoS_2 layer [Fig. 1(a)]. The zero energy is referenced to the valence band maximum at zero field. The bands are colored based on the projection of their wave functions onto the WS_2 and MoS_2 layers.
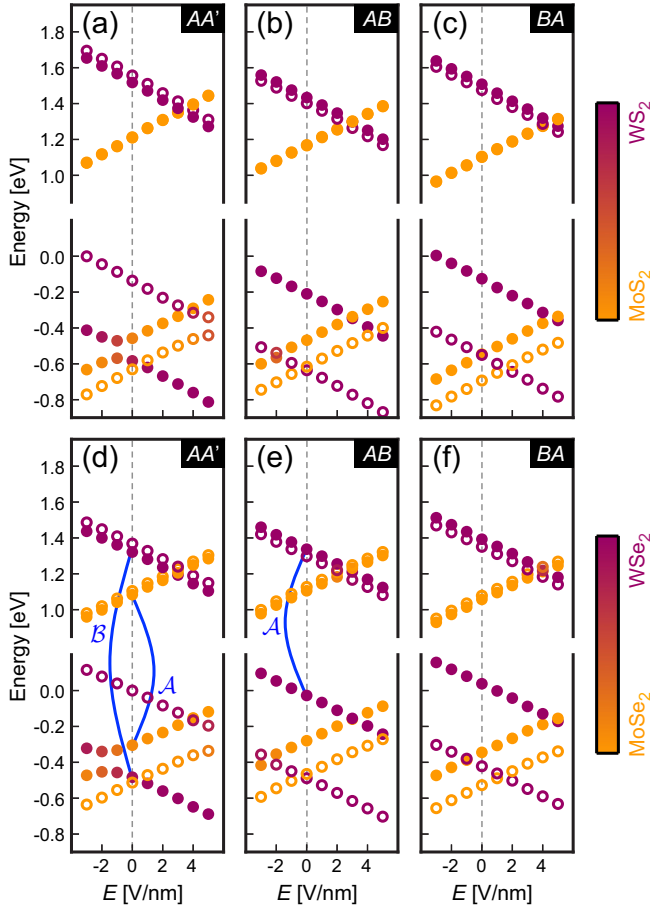
FIG. 3. Evolution of valence and conduction bands at K under a perpendicular electric field. Three stackings each are shown for (a)–(c) WS_2/MoS_2 and (d)–(f) $WSe_2/MoSe_2$. The zero energies of the WS_2/MoS_2 and $WSe_2/MoSe_2$ compounds are separately referenced to the valence band maximum of their AA' configurations at zero field. The filled (empty) circles denote states with majority up (down) spins, and are colored based on their wave function characters. The curves in panels (d) and (e) label intralayer $\mathcal{A}$ and $\mathcal{B}$ excitons that are discussed in the main text.

FIG. 4. (a), (b) Charge density isosurfaces of the valence and conduction band states at K in a monolayer of MoS_2. Side and top views are presented for each state. (c)–(f) Schematic depictions of possible interlayer hybridization of K states in AA'- and AB-stacked WS_2/MoS_2. Only the S atoms and their charge densities are shown for clarity (1 = MoS_2 layer, 2 = WS_2 layer). Interlayer hybridization is allowed when the wave functions on both layers transform identically under threefold rotation. The overlap appears largest in panel (c), where the lobes of charge density are directed towards each other.

Figure 3 shows the evolution of valence and conduction bands at K across a range of positive and negative electric fields, for all six heterobilayers considered. Away from crossings, the energies of WX_2-derived bands decrease linearly with electric field, while the energies of MoX_2-derived bands increase linearly with electric field. These results show clearly several important trends:

(i) Electrostatic inversion of the type II band alignment is possible, but requires large fields. The AB-stacked heterobilayers have the smallest critical fields, which are 3.0 V/nm for WS_2/MoS_2 and 3.1 V/nm for $WSe_2/MoSe_2$, based on linear fits to the spin-up bands.

(ii) The magnitudes of the slopes of the band energies versus field decrease in the order of WS_2-, MoS_2-, WSe_2-, and $MoSe_2$-derived bands. This trend is partly due to the greater polarizability of Se over S.

(iii) The distinction between AB and BA stacking being whether the W or Mo atoms are aligned with the X atoms of the opposite layer, th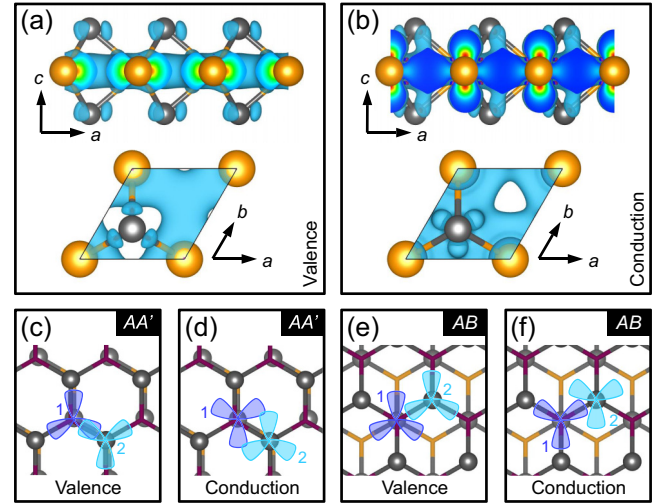ese two registries produce net dipole moments at zero field pointing in opposite directions. Thus, to first order, the BA plots are horizontal shifts of the AB plots by 1.7 V/nm for WS_2/MoS_2 and 1.4 V/nm for $WSe_2/MoSe_2$.

(iv) Away from crossings, the spin splittings remain relatively constant and are larger in magnitude for heavier elements.

(v) There is a sizable hybridization between valence bands of the same spin in the AA' heterobilayers. Smaller hybridizations can also occur when opposite-spin bands cross [for example, in Figs. 3(b) and 3(f)], but they are more difficult to observe due to our discrete sampling of electric field values.

To elucidate the origin of these effects, we consider the wave functions in the monolayer limit. Figures 4(a) and 4(b) show the charge density isosurfaces of the valence and conduction band states at K in a monolayer of MoS_2. Near the S atom, the valence band state has lobes directed along the bonds, whereas the conduction band state has lobes directed between the bonds. Based on Wannier transformations of DFT calculations [49], the state at the valence band maximum can be decomposed into $(d_{x^2-y^2} + id_{xy})$-like orbitals on the Mo atom and $(p_x + ip_y)$-like orbitals on the S atoms. Similarly, the state at the conduction band minimum can be decomposed into d_{z^2}-like orbitals on the Mo atom and $(p_x - ip_y)$-like orbitals on the S atoms. These states at K have $\mathcal{R}_3$ symmetry (threefold rotation): Under a counterclockwise rotation of $120°$ about the S atom, they acquire phase factors of $\exp(-i2\pi\mu/3)$, where $\mu = \pm1$ for the valence and conduction bands, respectively.

Generalizing to heterobilayers, we note that for AA', AB, and BA stacking configurations, $\mathcal{R}_3$ crystalline symmetry is maintained about each atomic site and is unaffected by a perpendicular electric field. Thus, for K states located on opposite layers to hybridize, their wave functions must

TABLE I. Symmetry-allowed hybridizations of valence ($\mathcal{V}$) and conduction ($\mathcal{C}$) bands that cross at K. The requisite spin characters from each layer are denoted by the arrows.

	AA'	AB	BA
$\mathcal{V}$	WX_2 ↑/MoX_2 ↑ WX_2 ↓/MoX_2 ↓	WX_2 ↓/MoX_2 ↑	WX_2 ↑/MoX_2 ↓
$\mathcal{C}$	WX_2 ↓/MoX_2 ↑	WX_2 ↓/MoX_2 ↑	WX_2 ↑/MoX_2 ↓

transform with the same phase factor under threefold rotation. For a given K state, counterclockwise rotation of $120°$ about a fixed atomic site engenders a phase factor of $\exp(i\phi)$, where

$$\phi = -\mathbf{K} \cdot \boldsymbol{\delta r} - \frac{2\pi\tau\mu}{3} - \frac{2\pi s_z}{3}. \tag{1}$$

The first term represents a Bloch phase, where $\mathbf{K} = \frac{4\pi}{3a}\hat{x}$ and $\boldsymbol{\delta r}$ is a displacement vector of the X atom that may arise from rotation. The second term, which was introduced in the previous paragraph, is generated by orbital angular momentum, with $\tau = \pm 1$ being the valley index. We note that $\tau = -1$ for the $180°$-oriented WX_2 layer in the AA' heterobilayers, and $+1$ otherwise. The third term is due to spin, with $s_z = \pm\frac{1}{2}$ for spins pointing in the positive or negative c direction. Using Eq. (1), we derive a set of hybridizations permitted by symmetry, shown in Table I. The actual strength of hybridization depends on matrix elements of the electric field operator and appears to be greatest in the valence bands of AA' heterobilayers. The stronger hybridization of these states could be due to a greater overlap of the charge densities near the X atoms facing the interlayer cavity [Figs. 4(c)–4(f)].

In what concerns direct excitons at K, our results imply that in the $0°$-stacked heterobilayers, the offset between the spin-up conduction bands defines an *upper bound* on the binding energy of interlayer excitons *relative* to that of the intralayer, WX_2 $\mathcal{A}$ exciton [15] [see Fig. 3(e)]. The actual binding energy of interlayer excitons is reduced due to the weaker Coulomb interaction between their spatially separated charges and varies depending on fabrication details [8,14,19]. Our results suggest that these energies can be tuned in two ways: First, by shifting the stacking registry from AB to BA, the spin-up, conduction band offset increases from 0.27 to 0.41 eV in WS$_2$/MoS$_2$ and

from 0.23 to 0.34 eV in WSe$_2$/MoSe$_2$ (DFT total energies for the AB and BA stackings are degenerate within 1 meV, suggesting that the configurations are equally stable). Second, by applying electric fields up to ± 1 V/nm, which are attainable in experiments involving dual-gated devices [50], the spin-up, conduction band offsets vary on average by ± 0.09 eV in WS$_2$/MoS$_2$ and ± 0.08 eV in WSe$_2$/MoSe$_2$.

In the $180°$-stacked heterobilayers, the large hybridization of valence bands at K should in principle affect the intralayer, WX_2 $\mathcal{B}$ exciton and the intralayer, MoX_2 $\mathcal{A}$ exciton [see Fig. 3(d)]. At zero field, the WX_2 $\mathcal{B}$ exciton can dissociate due to charge transfer from the spin-up WX_2 bands to the spin-up MoX_2 bands, so its PL signal may already be quenched. However, the MoX_2 $\mathcal{A}$ exciton cannot dissociate by hole transfer onto WX_2 without a spin flip, which is expected to occur rarely [17]; thus, its PL signal should be observable. As the system is tuned towards the hybridization point (near -1 V/nm for WS$_2$/MoS$_2$), we expect the recombination rate of the MoX_2 $\mathcal{A}$ exciton to drop. This is due to the hole sector of the excitonic wave function becoming spread over both layers, reducing its overlap with the electron sector that is confined to the MoX_2 layer [50]. Thus, valence band hybridization should lead to an observable darkening of the MoX_2 $\mathcal{A}$ exciton.

In summary, we report two effects of the stacking configuration that have impact on optoelectronic properties of WX_2/MoX_2 TMDC heterobilayers: First, relative shifts in the stacking registry can induce different net dipole moments, leading to band offset variations that affect the binding energy of interlayer excitons. Second, depending on the stacking configuration, a perpendicular electric field may hybridize WX_2 and MoX_2 bands that cross at K, darkening the intralayer excitons associated with these bands. We expect that these stacking effects may be enriched upon introduction of small twist angles about $0°$ or $180°$.

[1] A. K. Geim and I. V. Grigorieva, Nature (London) **499**, 419 (2013).

[2] K. F. Mak, C. Lee, J. Hone, J. Shan, and T. F. Heinz, Phys. Rev. Lett. **105**, 136805 (2010).

[3] A. Splendiani, L. Sun, Y. Zhang, T. Li, J. Kim, C.-Y. Chim, G. Galli, and F. Wang, Nano Lett. **10**, 1271 (2010).

[4] Q. H. Wang, K. Kalantar-Zadeh, A. Kis, J. N. Coleman, and M. S. Strano, Nat. Nanotechnol. **7**, 699 (2012).

[5] M. M. Furchi, A. Pospischil, F. Libisch, J. Burgdrfer, and T. Mueller, Nano Lett. **14**, 4785 (2014).

[6] X. Hong, J. Kim, S.-F. Shi, Y. Zhang, C. Jin, Y. Sun, S. Tongay, J. Wu, Y. Zhang, and F. Wang, Nat. Nanotechnol. **9**, 682 (2014).

[7] F. Ceballos, M. Z. Bellus, H.-Y. Chiu, and H. Zhao, ACS Nano **8**, 12717 (2014).

[8] Y. Yu, S. Hu, L. Su, L. Huang, Y. Liu, Z. Jin, A. A. Purezky, D. B. Geohegan, K. W. Kim, Y. Zhang, and L. Cao, Nano Lett. **15**, 486 (2015).

[9] M.-H. Chiu, C. Zhang, H.-W. Shiu, C.-P. Chuu, C.-H. Chen, C.-Y. S. Chang, C.-H. Chen, M.-Y. Chou, C.-K. Shih, and L.-J. Li, Nat. Commun. **6**, 7666 (2015).

[10] A. F. Rigosi, H. M. Hill, Y. Li, A. Chernikov, and T. F. Heinz, Nano Lett. **15**, 5033 (2015).

[11] C.-H. Lee, G.-h. Lee, A. M. van der Zande, W. Chen, Y. Li, M. Han, X. Cui, G. Arefe, C. Nuckolls, T. F. Heinz, J. Guo, J. Hone, and P. Kim, Nat. Nanotechnol. **9**, 676 (2014).

[12] H. Fang, C. Battaglia, C. Carraro, S. Nemsak, B. Ozdol, J. S. Kang, H. A. Bechtel, S. B. Desai, F. Kronast, A. A. Unal, G. Conti, C. Conlon, G. K. Palsson, M. C. Martin, A. M. Minor,

C. S. Fadley, E. Yablonovitch, R. Maboudian, and A. Javey, Proc. Natl. Acad. Sci. USA **111**, 6198 (2014).

[13] M.-H. Chiu, M.-Y. Li, W. Zhang, W.-T. Hsu, W.-H. Chang, M. Terrones, H. Terrones, and L.-J. Li, ACS Nano **8**, 9649 (2014).

[14] Y. Gong, J. Lin, X. Wang, G. Shi, S. Lei, Z. Lin, X. Zou, G. Ye, R. Vajtai, B. I. Yakobson, H. Terrones, M. Terrones, B. K. Tay, J. Lou, S. T. Pantelides, Z. Liu, W. Zhou, and P. M. Ajayan, Nat. Mater. **13**, 1135 (2014).

[15] P. Rivera, J. R. Schaibley, A. M. Jones, J. S. Ross, S. Wu, G. Aivazian, P. Klement, K. Seyler, G. Clark, N. J. Ghimire, J. Yan, D. G. Mandrus, W. Yao, and X. Xu, Nat. Commun. **6**, 6242 (2015).

[16] Y. Gong, S. Lei, G. Ye, B. Li, Y. He, K. Keyshar, X. Zhang, Q. Wang, J. Lou, Z. Liu, R. Vajtai, W. Zhou, and P. M. Ajayan, Nano Lett. **15**, 6135 (2015).

[17] P. Rivera, K. L. Seyler, H. Yu, J. R. Schaibley, J. Yan, D. G. Mandrus, W. Yao, and X. Xu, Science **351**, 688 (2016).

[18] Y. He, Y. Yang, Z. Zhang, Y. Gong, W. Zhou, Z. Hu, G. Ye, X. Zhang, E. Bianco, S. Lei, Z. Jin, X. Zou, Y. Yang, Y. Zhang, E. Xie, J. Lou, B. Yakobson, R. Vajtai, B. Li, and P. Ajayan, Nano Lett. **16**, 3314 (2016).

[19] S. Tongay, W. Fan, J. Kang, J. Park, U. Koldemir, J. Suh, D. S. Narang, K. Liu, J. Ji, J. Li, R. Sinclair, and J. Wu, Nano Lett. **14**, 3185 (2014).

[20] A. Chernikov, A. M. van der Zande, H. M. Hill, A. F. Rigosi, A. Velauthapillai, J. Hone, and T. F. Heinz, Phys. Rev. Lett. **115**, 126802 (2015).

[21] M. M. Fogler, L. V. Butov, and K. S. Novoselov, Nat. Commun. **5**, 4555 (2014).

[22] A. Ramasubramaniam, D. Naveh, and E. Towe, Phys. Rev. B **84**, 205325 (2011).

[23] Q. Liu, L. Li, Y. Li, Z. Gao, Z. Chen, and J. Lu, J. Phys. Chem. C **116**, 21556 (2012).

[24] E. J. G. Santos and E. Kaxiras, ACS Nano **7**, 10741 (2013).

[25] Z. Y. Zhang, M. S. Si, Y. H. Wang, X. P. Gao, D. Sung, S. Hong, and J. He, J. Chem. Phys. **140**, 174707 (2014).

[26] J. Xiao, M. Long, X. Li, Q. Zhang, H. Xu, and K. Chan, J. Phys.: Condens. Matter **26**, 405302 (2014).

[27] N. Zibouche, P. Philipsen, A. Kuc, and T. Heine, Phys. Rev. B **90**, 125440 (2014).

[28] K. V. Shanavas and S. Satpathy, Phys. Rev. B **91**, 235145 (2015).

[29] C. V. Nguyen, N. N. Hieu, and V. V. Ilyasov, J. Electron. Mater. **45**, 4038 (2016).

[30] N. Lu, H. Guo, L. Li, J. Dai, L. Wang, W.-N. Mei, X. Wu, and X. C. Zeng, Nanoscale **6**, 2879 (2014).

[31] M. Sharma, A. Kumar, P. K. Ahluwalia, and R. Pandey, J. Appl. Phys. **116**, 063711 (2014).

[32] G. Kresse and J. Furthmüller, Comp. Mater. Sci. **6**, 15 (1996).

[33] G. Kresse and J. Furthmüller, Phys. Rev. B **54**, 11169 (1996).

[34] P. E. Blöchl, Phys. Rev. B **50**, 17953 (1994).

[35] G. Kresse and D. Joubert, Phys. Rev. B **59**, 1758 (1999).

[36] J. P. Perdew, K. Burke, and M. Ernzerhof, Phys. Rev. Lett. **77**, 3865 (1996).

[37] J. Neugebauer and M. Scheffler, Phys. Rev. B **46**, 16067 (1992).

[38] G. Makov and M. C. Payne, Phys. Rev. B **51**, 4014 (1995).

[39] See Supplemental Material at http://link.aps.org/supplemental/10.1103/PhysRevB.94.241303 for further computational details involving structural features of heterobilayers, van der Waals correction, and artificial vacuum states.

[40] A. Tkatchenko and M. Scheffler, Phys. Rev. Lett. **102**, 073005 (2009).

[41] T. Bučko, S. Lebègue, J. Hafner, and J. G. Ángyán, Phys. Rev. B **87**, 064110 (2013).

[42] G. Constantinescu, A. Kuc, and T. Heine, Phys. Rev. Lett. **111**, 036104 (2013).

[43] H. Yu, Y. Wang, Q. Tong, X. Xu, and W. Yao, Phys. Rev. Lett. **115**, 187002 (2015).

[44] M. M. Ugeda, A. J. Bradley, S.-F. Shi, F. H. da Jornada, Y. Zhang, D. Y. Qiu, W. Ruan, S.-K. Mo, Z. Hussain, Z.-X. Shen, F. Wang, S. G. Louie, and M. F. Crommie, Nat. Mater. **13**, 1091 (2014).

[45] H. M. Hill, A. F. Rigosi, K. T. Rim, G. W. Flynn, and T. F. Heinz, Nano Lett. **16**, 4831 (2016).

[46] K. Kośmider and J. Fernández-Rossier, Phys. Rev. B **87**, 075451 (2013).

[47] L. Debbichi, O. Eriksson, and S. Lebègue, Phys. Rev. B **89**, 205311 (2014).

[48] Y. Liang, S. Huang, R. Soklaski, and L. Yang, Appl. Phys. Lett. **103**, 042106 (2013).

[49] S. Fang, R. Kuate Defo, S. N. Shirodkar, S. Lieu, G. A. Tritsaris, and E. Kaxiras, Phys. Rev. B **92**, 205108 (2015).

[50] T. Chu, H. Ilatikhameneh, G. Klimeck, R. Rahman, and Z. Chen, Nano Lett. **15**, 8000 (2015).

[51] K. Momma and F. Izumi, J. Appl. Crystallogr. **44**, 1272 (2011).